IEEE Access
Multidisciplinary | Rapid Review | Open Access Journal

Received January 11, 2019, accepted January 21, 2019, date of publication January 31, 2019, date of current version February 14, 2019.

Digital Object Identifier 10.1109/ACCESS.2019.2895413

An Accurate Vehicle and Road Condition Estimation Algorithm for Vehicle Networking Applications

HUIYUAN XIONG[1,2,3], JIANXUN LIU[1], RONGHUI ZHANG[1,3], XIONGLAI ZHU[1], AND HUAN LIU[1]

[1]School of Intelligent Systems Engineering, Sun Yat-sen University, Guangzhou 510006, China
[2]Institute of Dongguan, Sun Yat-sen University, Dongguan 523808, China
[3]Guangdong Key Laboratory of Intelligent Transportation System, Sun Yat-sen University, Guangzhou 510275, China

Corresponding author: Ronghui Zhang (zrh1981819@126.com)

This work was supported in part by the National Natural Science Foundation of China under Grant 51775565, in part by the Natural Science and Technology Special Projects under Grant 2018-1521, in part by the Major Science and Technology Special Projects in Guangdong under Grant 2016B010118001, and in part by the Fundamental Research Funds for the Central Universities under Grant 18lgpy83.

ABSTRACT The Internet of Vehicles is essential for building smart cities. By analyzing the big data collected by vehicle sensors on the road, we can estimate vehicle information and real-time road conditions. To improve the prediction accuracy, this paper proposes a new adaptive filtering algorithm for variable measurement noise problems that occur during the driving state estimations of two-axle electric vehicles. Based on the nonlinear three-degree-of-freedom vehicle model, the dual-motor torque output model, and the Dugoff tire model, fuzzy logic is used to correct the measurement noise in the cubature Kalman filter algorithm. Moreover, the ant colony algorithm is used to optimize the input and output membership functions. Based on the big sensor data, we can accurately predict road conditions, such as vehicle speed and road adhesion coefficients. The simulation results based on CarSim/Simulink show that the new algorithm improves the estimation accuracy of the whole system, regardless of whether the measurement noise is fixed or variable. The research in this paper provides a reference for multi-data comprehensive analyses under different vehicle states.

INDEX TERMS Big sensor data, ant colony algorithm, fuzzy control, cubature Kalman filter, state estimation.

I. INTRODUCTION

In today's big data and widely interconnected society, as a result of the rapid development of urban processes, big traffic data and the Internet of Vehicles have become a key weapon in urban management. Acquiring and processing big traffic data is essential to urban planning and digital city constructions. Many scholars have investigated these fields. A long-term traffic anomaly detection method and a new two-stage method [1], [2] were proposed to obtain road traffic conditions for optimal path predictions. Articles [3]–[7] propose an adaptive and scalable energy-aware algorithm for mobile big data offloading environments. Articles [8]–[10] propose a spatiotemporal big data analysis method. Articles [11]–[13] address the integration of Internet of Things (IoT) and Internet of Vehicles (IoV) for the physical and social layer information of rapid content transmission from device to device and vehicle to vehicle (D2D-V2V).

Vehicle information collection and uploading is an important basis for the above technology. Electric vehicles will become the main form of future cars. However, the structural characteristics of electric vehicles are slightly different from those of traditional cars. In paper [14], a numerical simulation of the regenerative braking torque distribution strategy was developed for the electric vehicle braking energy feedback control. Articles [15], [16] analyze the social behaviors and mobilities of urban traffic nodes based on the expected application of VSN and communication architecture. Articles [17], [18] relate to electric vehicle battery storage management systems that can be applied to smart cities and vehicle networking applications. Article [19] proposes the social welfare data collection framework for collecting data

The associate editor coordinating the review of this manuscript and approving it for publication was Xiangjie Kong.

generated by smart devices and forwarding them to a data center; the purpose of this framework is to achieve intelligent driving and traffic planning.

In articles [20]–[22], we considered a mobile data offloading system that integrates cellular networks and onboard opportunity communications. Articles [23]–[25] propose a novel architecture for real-time ITS big data analysis in an IoV environment. In articles [26]–[30], due to the extended sensing range, we can explicitly consider the behavioral correlation between multiple vehicles in the Internet of Vehicles. Then, we can infer the motion intention of each vehicle. Article [31] proposes a binocular stereo vision (BSV) system, which provides a basis for automotive sensing applications.

To better improve the accuracy of dealing with uploaded data, we must make timely estimates of the vehicle information and real-time road conditions through the sensor information from cars. Considering the cost and practical performance of sensors, most of the current production models mainly estimate some key parameters during the state estimation. Articles [32]–[38] use the unscented Kalman filter (UKF) to estimate the whole vehicle system and nonlinear tire force. The author of these studies proposes a new method to solve the vehicle state problem in the Internet of Vehicles. In paper [39], based on the optimal robust control algorithm and servo-loop control algorithm, the vehicle brake actuator is improved, and the tracking accuracy is optimized. Article [40] proposes a method to improve the performance of a nonlinear suspension system under primary resonance conditions. The results show that the relative displacement response can be effectively suppressed. In addition, the jump of the hardened and softened primary isolators can be eliminated. Articles [17], [41]–[45], [52] proposed a three-degree-of-freedom vehicle dynamics model in which the Dugoff tire model was applied. As a result, the position estimation of the new model was more accurate than those using GPS. Article [41], [46]–[49] proposes a new method for estimating the tire force of a vehicle and the maximum adhesion of the road.

But in fact, the above methods are not always satisfactory in practical applications. Vehicle dynamics modeling often has unavoidable errors in the actual system, which means that the model cannot fully reflect the real physical processes of the vehicle or the road condition. Therefore, compared with the traditional extended Kalman filter, unscented Kalman, least squares and other vehicle state estimation methods, the accuracy of cubature Kalman filter estimation is relatively higher, and its real-time performance is stronger. However, the existing cubature Kalman filter state observers use the noise covariance as a known constant in the filtering process, which is contrary to the actual road conditions. In this paper, to obtain the state information of the two-axle electric vehicle and road condition estimation, we propose an adaptive estimation algorithm based on an ant colony optimization fuzzy logic cubature Kalman filter. This algorithm has higher stability, robustness, better real-time performance, and improved estimation accuracy of road state variables. This provides a reference for application of IoV in smart cities.

The rest of this paper is organized as follows. In Section II, we elaborate the theoretical basis of the three-degree-of-freedom vehicle model, dual motor torque output model, and Dugoff tire model. In Section III, we illustrate the two-axis driven electric vehicle driving state estimation and road surface state estimation based on the cubature Kalman filtering algorithm. In Section III, we explain and derive the fuzzy cubature Kalman algorithm and ACO-based membership function optimization. In Section IV, we conduct software simulations and results analysis. Finally, in Section V, we summarize the conclusions and propose future work.

II. VEHICLE DYNAMICS MODEL

A. THREE-DEGREE-OF-FREEDOM VEHICLE MODEL

In this paper, we only consider yaw, longitudinal, and lateral movements to estimate the model more concisely and efficiently. At the same time, we make the following assumptions:

(1) We ignored the effect of rolling resistance when estimating vehicle state parameters;
(2) The entire suspension system does not affect the vertical movement of the car;
(3) We do not consider the degree of freedom of the car's pitch and roll directions.

The established three-degree-of-freedom vehicle dynamics model is shown in FIGURE 1.

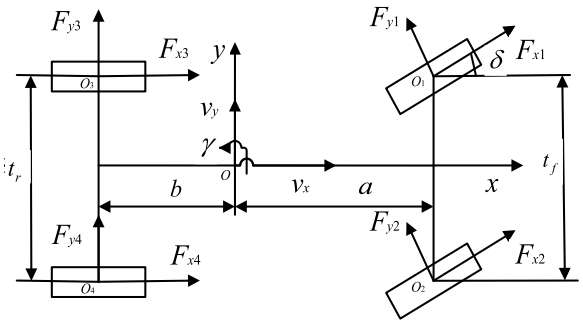

FIGURE 1. Three-degree-of-freedom vehicle dynamics model.

The differential equations of the three-degree-of-freedom vehicle dynamics model are as follows:

The differential equation of longitudinal motion:

$$\dot{v}_x = a_x + \gamma \cdot v_y \tag{1}$$

The differential equation of lateral motion:

$$\dot{v}_y = a_y + \gamma \cdot v_x \tag{2}$$

The differential equation of yaw motion:

$$\begin{aligned}\dot{\gamma} = \Big[& a\left(F_{x1} + F_{x2}\right)\sin\delta + a\left(F_{y1} + F_{y2}\right)\cos\delta \\ & -b\left(F_{y3} + F_{y4}\right) - \frac{t_f}{2}\left(F_{x1} - F_{x2}\right)\cos\delta \\ & + \frac{t_f}{2}\left(F_{y1} - F_{y2}\right)\sin\delta - \frac{t_r}{2}\left(F_{x3} - F_{x4}\right)\Big]/I_Z\end{aligned} \tag{3}$$

where a_x is the longitudinal acceleration at the barycenter of the car and a_y is the lateral acceleration of the car's barycenter; v_x and v_y are the longitudinal and lateral velocities at the barycenter, respectively; γ is the angular velocity of the yaw; t_f and t_r are the wheelbases of the front and rear wheels, respectively; a is the distance from centroid to the front axle, and b is the distance from centroid to the rear axle; F_{xi} and F_{yi} are the longitudinal and lateral forces on each wheel, respectively, where $i = 1, 2, 3, 4$ represent the left front wheel, the right front wheel, the left rear wheel, and the right rear wheel, respectively; δ is the front wheel steering angle; and I_Z is the moment of inertia of the whole vehicle around the vertical axis.

B. DUAL MOTOR TORQUE OUTPUT MODEL

Compared with the traditional single-motor-driven electric vehicle, the front and rear axle dual-motor drive structure can increase the power of the vehicle. Moreover, the dual-motor drive structure can improve the utilization efficiency of a single motor under the same working conditions, which improves the driving performance of the whole vehicle. The dual-motor drive structure effectively optimizes the space utilization of the vehicle and enhances flexibility during vehicle operation. The driving equation of the dual-motor drive structure is as follows:

$$J_w \cdot \dot{\omega}_i = T_{di} - F_{xi} \cdot R_v \tag{4}$$

where J_w is the moment of inertia of the wheel; ω_i(i = 1, 2, 3, 4) is the angular velocity of each wheel; T_{di} is the driving torque acting on the wheel; and R_v is the wheel rolling radius.

In this paper, we equate the wheel rotation equations on the left and right sides of the car to the midpoint of the front and rear axles, and then we convert the wheel drive torque into front and rear motor output torque. The equations are as follows:

$$\dot{\omega}_{rc} = max\left(\omega_3, \omega_4\right)' = \frac{1}{2J_w}\left(T_{mr} i_t \eta_t - F_{xr} R_v\right) \tag{5}$$

$$\dot{\omega}_{fc} = max\left(\omega_1, \omega_2\right)' = \frac{1}{2J_w}\left(T_{mf} i_t \eta_t - F_{xf} R_v\right) \tag{6}$$

where $\omega_1, \omega_2, \omega_3, and\ \omega_4$ are the rotational speeds of the left front wheel, the right front wheel, the left rear wheel, and the right rear wheel, respectively; ω_{fc} and ω_{rc} are the equivalent rotational angular velocities at the midpoint of the front and rear axles, respectively; F_{xf} and F_{xr} are the ground longitudinal reaction forces received by the front and rear axles, respectively; T_{mf} is the driving torque of the front axle motor; T_{mr} is the driving torque of the rear axle motor; i_t is the total transmission ratio of the transmission system; and η_t is the total transmission efficiency.

C. DUGOFF TIRE MODEL

In this paper, we use a Dugoff tire model to simplify the estimation process. The longitudinal force and lateral force expression formulas acting on each tire are as follows:

$$F_{xi} = \mu \cdot F_{zi} \cdot C_x \cdot \frac{s_i}{1 - s_i} \cdot f\left(L\right) \tag{7}$$

$$F_{yi} = \mu \cdot F_{zi} \cdot C_y \cdot \frac{\tan \alpha_i}{1 - s_i} \cdot f\left(L\right) \tag{8}$$

$$f\left(L\right) = \begin{cases} L\left(2 - L\right), & L < 1 \\ 1, & L \geq 1 \end{cases} \tag{9}$$

$$L = \frac{\left(1 - s_i\right)\left(1 - \varepsilon v_x \sqrt{C_x^2 s_i^2 + C_y^2 \tan \alpha_i^2}\right)}{2 \cdot \sqrt{C_x^2 s_i^2 + C_y^2 \tan \alpha_i^2}} \tag{10}$$

where $F_{zi}(i = 1, 2, 3, 4)$ is the vertical load of each tire; μ is the current road adhesion coefficient; $s_i(i = 1, 2, 3, 4)$ is the longitudinal slip ratio; α_i is the tire side angle; ε is the speed influence factor; C_x, C_y are the longitudinal stiffness and the lateral stiffness of the tire, respectively; and L is the introduced boundary condition.

According to the definition of the slip ratio in automobile theory, in the case of driving, the slip ratio can be expressed as follows:

$$s_i = \frac{R_v \omega_i - v_x}{R_v \omega_i} = 1 - \frac{v_x}{R_v \omega_i} > 0 \tag{11}$$

In the case of braking, the slip ratio can be expressed as follows:

$$s_i = \frac{R_v \omega_i - v_x}{v_x} = \frac{R_v \omega_i}{v_x} - 1 < 0 \tag{12}$$

III. TWO-AXIS DRIVING ELECTRIC VEHICLE DRIVING STATE ESTIMATION

A. CUBATURE KALMAN FILTERING ALGORITHM

The cubature Kalman filtering algorithm [50] is a Bayesian filtering algorithm based on spherical radial integral. The cubature Kalman filtering algorithm was proposed by Arasaratnam et al. in 2009, and its specific implementation steps are as follows:

(1) Initialize the estimated value $\hat{\boldsymbol{x}}_0$ and error covariance P_0:

$$\hat{\boldsymbol{x}}_0 = E\left[x_0\right] \tag{13}$$

$$P_0 = E\left[\left(x_0 - \hat{\boldsymbol{x}}_0\right)\left(x_0 - \hat{\boldsymbol{x}}_0\right)^T\right] \tag{14}$$

(2) Update the time:

- Cholesky decomposition of error covariance $\boldsymbol{P}_{k\lfloor k}$:

$$\boldsymbol{P}_{k\lfloor k} = \boldsymbol{S}_{k\lfloor k} \boldsymbol{S}_{k\lfloor k}^{\mathrm{T}} \tag{15}$$

$$\mathrm{X}_{\mathrm{i,k\lfloor k}} = \mathrm{S}_{\mathrm{k\lfloor k}} \xi_{\mathrm{i}} + \hat{\boldsymbol{x}}_{\mathrm{k\lfloor k}} \tag{16}$$

  where $\boldsymbol{S}_{k\lfloor k}$ is the square root of $\boldsymbol{P}_{k\lfloor k}$; $\boldsymbol{X}_{i,k\lfloor k}$ is the calculated cubature point; and $\boldsymbol{\xi}_i = \sqrt{n}\left[1\right]_i$, where n is the state dimension and $\left[1\right]_i$ is the basic cubature point.
- Output the cubature point $\boldsymbol{X}^*_{i,k+1\lfloor k}$:

$$X^*_{i,k+1\lfloor k} = f\left(X_{i,k\lfloor k}, u_k\right) \tag{17}$$

- State prediction value $\hat{\boldsymbol{x}}_{k+1|k}$:

$$\hat{\boldsymbol{x}}_{k+1|k} = \frac{1}{2n}\sum_{i=1}^{2n}\boldsymbol{X}^{*}_{i,k+1\lfloor k} \tag{18}$$

- Covariance prediction $\hat{P}_{k+1\lfloor k}$:

$$\hat{P}_{k+1\lfloor k} = \frac{1}{2n}\sum_{i=1}^{2n}\boldsymbol{X}^{*}_{\mathrm{i,k+1\lfloor k}}\left(\sum_{i=1}^{2n}\boldsymbol{X}^{*}_{i,k+1\lfloor k}\right)^{T} - \hat{\boldsymbol{x}}_{k+1|k}\left(\hat{\boldsymbol{x}}_{k+1|k}\right)^{T} + Q \tag{19}$$

(3) Update the measurements:

- Cholesky decomposition of error covariance $\boldsymbol{P}_{\mathrm{k+1\lfloor k}}$:

$$\boldsymbol{P}_{k+1\lfloor k} = \boldsymbol{S}_{k+1\lfloor k}\boldsymbol{S}^{T}_{k+1|k} \tag{20}$$

$$\boldsymbol{X}_{i,k+1\lfloor k} = \boldsymbol{S}_{k+1\lfloor k}\xi_i + \hat{\boldsymbol{x}}_{k+1|k} \tag{21}$$

- Propagation cubature point $\boldsymbol{Z}_{i,k+1\lfloor k}$:

$$\boldsymbol{Z}_{i,k+1\lfloor k} = h\left(\boldsymbol{X}_{i,k+1\lfloor k}, \boldsymbol{u}_k\right) \tag{22}$$

- Measurement prediction $\hat{z}_{k+1|k}$:

$$\hat{z}_{k+1|k} = \frac{1}{2n}\sum\nolimits_{i=1}^{2n} Z^{*}_{i,k+1\lfloor k} \tag{23}$$

- New interest covariance $\hat{P}_{zz,k+1\lfloor k}$:

$$\hat{P}_{zz,k+1\lfloor k} = \frac{1}{2n}\sum_{i=1}^{2n} Z_{i,k+1\lfloor k}\left(Z_{i,k+1\lfloor k}\right)^{T} - \hat{z}_{k+1|k}\left(\hat{z}_{k+1|k}\right)^{T} + R \tag{24}$$

- Cross-covariance variance $\hat{P}_{xz,k+1\lfloor k}$:

$$\hat{P}_{xz,k+1\lfloor k} = \frac{1}{2n}\sum_{i=1}^{2n} X_{i,k+1\lfloor k}\left(Z_{i,k+1\lfloor k}\right)^{T} - \hat{\boldsymbol{x}}_{k+1|k}\left(\hat{z}_{k+1|k}\right)^{T} \tag{25}$$

- Gain matrix $\boldsymbol{K}_{k+1}$:

$$\boldsymbol{K}_{k+1} = \boldsymbol{P}_{xz,k+1\lfloor k}\boldsymbol{P}^{-1}_{zz,k+1\lfloor k} \tag{26}$$

- State variables $\hat{\boldsymbol{x}}_{k+1|k+1}$:

$$\hat{\boldsymbol{x}}_{k+1|k+1} = \hat{\boldsymbol{x}}_{k+1|k} + \boldsymbol{K}_{k+1}\left(z_{k+1} - \hat{z}_{k+1|k}\right) \tag{27}$$

- Error covariance $\boldsymbol{P}_{k+1\lfloor k+1}$:

$$\boldsymbol{P}_{k+1\lfloor k+1} = \boldsymbol{P}_{k+1\lfloor k} - \boldsymbol{K}_{k+1}\boldsymbol{P}_{zz,k+1\lfloor k}\boldsymbol{K}^{\mathrm{T}}_{k+1} \tag{28}$$

Referring to the three-degree-of-freedom vehicle dynamics model and the Dugoff tire model established in the previous section, we establish state space equations after discretizing the nonlinear vehicle system. The equations are as follows:

$$\begin{cases} x_{k+1} = f\left(x_k, u_k, w_k\right) \\ z_k = h\left(x_k, v_k\right) \end{cases} \tag{29}$$

where $\boldsymbol{w}_k$ and $\boldsymbol{v}_k$ are the process noise and measurement noise, respectively, which are uncorrelated in the filtering process and follow a Gaussian distribution. We define the covariance of process noise and measurement noise as $\boldsymbol{Q}$ and $\boldsymbol{R}$, respectively, and their values are as follows:

$$Q = diag\left[r_{11}, r_{22}, r_{33}, r_{44}, r_{55}, r_{66}\right]$$
$$R = diag\left[k_{11}, k_{22}, k_{33}\right]$$

In this paper, we use the values of $a_x, a_y, \gamma, and\,\delta$ and the wheel speed information $\omega_1, \omega_2, \omega_3, and\,\omega_4$ obtained by the sensor to estimate the values of $v_x, v_y, \gamma, and\,\mu$ according to the system control algorithm. Therefore, the state variable in the equation is $x_k = \left[v_x, v_y, a_x, a_y, \gamma, \mu\right]$, the system control input is $u_k = [\omega_i, \gamma]$, and the observation output vector is $z_k = \left[a_x, a_y, \gamma\right]$. The purpose of setting the yaw angle to the estimated value is to make better use of the measured information and to improve the reliability of the estimation. The purpose of setting the adhesion coefficient to the estimated value is to enable the entire estimation model to obtain the road surface condition.

B. FUZZY CUBATURE KALMAN ALGORITHM

In the process of estimating the vehicle state using the conventional cubature Kalman filter algorithm, the noise covariance matrices $\boldsymbol{Q}$ and $\boldsymbol{R}$ are constant matrices. The measurement noise covariance matrix $\boldsymbol{R}$ is an important parameter in the filtering process. If the measurement noise covariance $\boldsymbol{R}$ is unreasonable, the filtering effect will not achieve the desired effect. If the value of $\boldsymbol{R}$ is too large, the algorithm may diverge. Otherwise, the convergence may occur too early. In the cubature Kalman filter algorithm, the process noise $\boldsymbol{Q}$ itself has good robustness after compensation. Therefore, the actual estimation of $\boldsymbol{Q}$ is relatively less meaningful. In this paper, we mainly adjust the system measurement noise $\boldsymbol{R}$ through fuzzy logic control to achieve adaptive adjustment of the filter. Moreover, we assume that the measurement noise covariance matrix of the system at time k is $\boldsymbol{R}_k$, where $\boldsymbol{R}_k = n\cdot\boldsymbol{R}_{k-1}$. We also ignore the estimation of $\boldsymbol{Q}_k$ to obtain a faster and more efficient algorithm.

The specific steps of the fuzzy cubature Kalman filter (FCKF) designed in this paper are as follows:

(1) Define the difference e_k between the innovation actual variance and the theoretical variance at time k, and e_k will be used as the input to the fuzzy controller:

$$e_k = \delta_r - \delta_t \tag{30}$$

where $\delta_r = \hat{Z}_{k\lfloor k-1}\left(\hat{Z}_{k\lfloor k-1}\right)^{T}$ is the innovation actual variance and $\delta_t = H_k P_{k\lfloor k-1}H^{T} + R_k$ is the innovation theoretical variance.

(2) In consideration of the final output of the fuzzy controller as the adjustment amount, the following fuzzy rules are defined.

a) If the innovation actual variance is greater than the theoretical variance (i.e., $e_k > 0$), then decrease δ_r;

b) If the innovation actual variance is approximately equal to the theoretical variance (i.e., $e_k \approx 0$), then do not change δ_r;

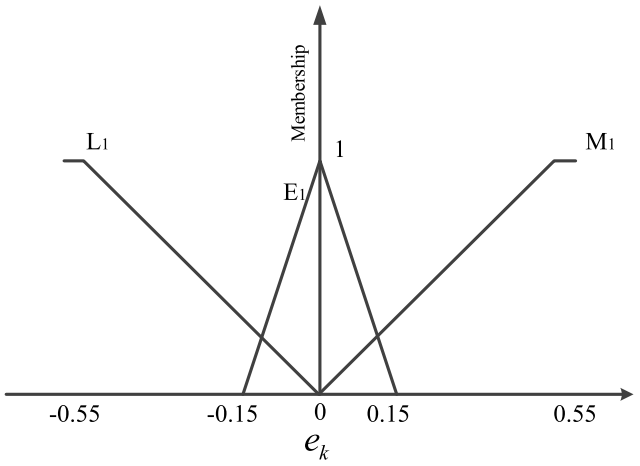

FIGURE 2. Membership function of input variable.

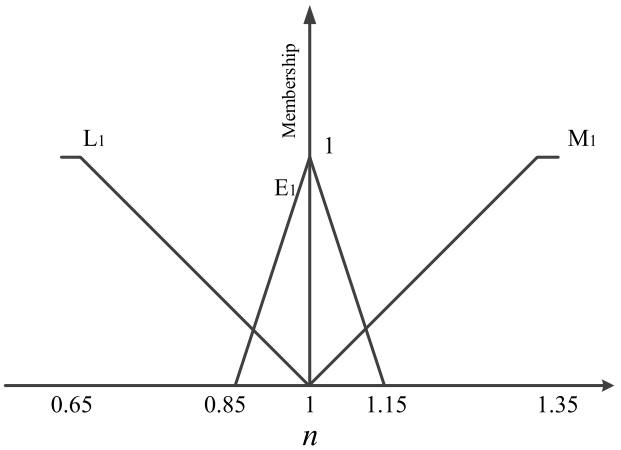

FIGURE 3. Membership function of output variable.

c) If the innovation actual variance is less than the theoretical variance (i.e., $e_k < 0$), then increase δ_r.

(3) Establish the membership function which is shown in FIGURE 2 and FIGURE 3.

C. ACO-BASED MEMBERSHIP FUNCTION OPTIMIZATION

In fuzzy control, it is often necessary to continuously test and summarize the control rules. Therefore, the membership function, as a variable, can be adjusted to the optimal state. In this paper, we use the ant colony algorithm [51] to optimize the membership function. The purpose is to increase the adaptability of the whole vehicle state parameter estimation system and improve the estimation accuracy of the cubature Kalman filter.

The ant colony optimization algorithm is a heuristic global optimization method proposed by Italian scholar Dorigo. The algorithm is based on the path selection phenomenon of ant foraging. At time t, the probability that ant p will transfer from position i to position j is as follows:

$$M_{ij(t)} = \begin{cases} \dfrac{\tau_{ij}^{a}(t)\,\eta_{ij}^{\theta_0}(t)}{\sum\limits_{r\in A}\tau_{ir}^{\alpha}(t)\,\eta_{ir}^{\theta_0}(t)}, & (j \in A) \\ 0, (others) \end{cases} \tag{31}$$

TABLE 1. Vehicle model parameters.

Variable parameter	Numerical value
Vehicle quality/*kg*	1643
Distance from centroid to front axle/*m*	1.287
Distance from centroid to rear axle/*m*	1.403
Front wheel track/*m*	1.581
Rear wheel track/*m*	1.586
Wheel rolling radius/*m*	0.359
Centroid height/*m*	0.545
Moment of inertia around the z-axis/$kg.m^2$	1954

where τ_{ij}(t) is the pheromone trajectory strength of ant p near the neighborhood of position i at time t; η_{ij} (t) is the degree of inspiration for ant p to move from position i to position j; α indicates the relative importance of the trajectory; θ_0 is the relative importance of visibility; r is the location that the ant can reach; and A is the set of locations that ant p can choose next.

After a cycle, the pheromone intensity of the ant colony on each path is updated in real time according to the following formula at time (t+1):

$$\begin{cases} \tau_{ij}(t+1) = (1-\rho)\,\tau_{ij}(t) + \Delta\tau_{ij}(t) \\ \Delta\tau_{ij}(t) = \sum_{P}^{N}\Delta\tau_{ij}^{p}(t) \end{cases} \tag{32}$$

where ρ is the pheromone residual coefficient ($0 \le \rho < 1$); $1-\rho$ represents the volatility of the pheromone; and $\Delta\tau_{ij}^{p}(t)$ is the pheromone released by ant p between position i and position j in this cycle. The shorter the path of ant p is between two select locations, the greater the amount of pheromone that is released.

The selected input and output membership function must be as accurate as possible. These two functions directly affect the adaptive adjustment factor n. In this paper, we use ACO to optimize the selected membership function. The direct goal of optimization is to find the optimal value at the lower vertex of the triangle membership function to obtain the best input and output membership function. The objective function determined by the difference between the actual variance of the innovation and the theoretical variance is as follows:

$$f_{obj} = 1/(1+e_k) \tag{33}$$

The specific implementation process is shown in FIGURE 4.

By using ACO to optimize the input and output membership functions, we can derive the optimal input and output

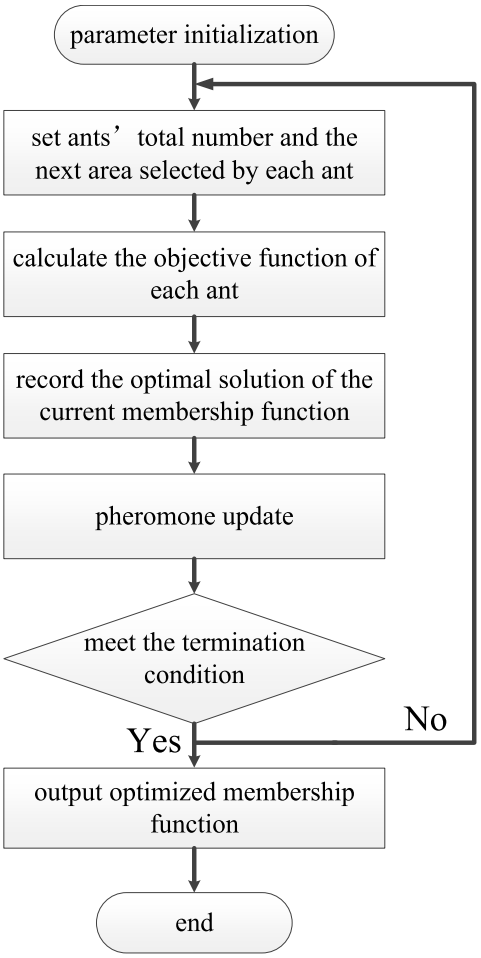

FIGURE 4. Optimization flow chart of membership function.

of the lower vertices of the triangle membership function. Therefore, we can increase the precision of the adaptive adjustment factor n and finally increase the filtering accuracy.

IV. SIMULATION VERIFICATION

A. DETERMINATION OF THE OPTIMAL MEMBERSHIP FUNCTION

For the input and output membership functions, multiple offline simulation tests are needed to test the superiority of the membership function at different noise levels. The purpose of introducing ACO is to obtain a better membership function and apply it to the measurement noise filtering process with time series variation, which increases the accuracy of the whole state estimation algorithm.

We first built a CarSim/Simulink dual-axis drive electric vehicle system state estimation joint simulation platform in the MATLAB/Simulink environment. The parameters of the vehicle model selected in the simulation are shown in TABLE I.

A schematic diagram of the joint simulation of CarSim/Simulink for a two-axis drive electric vehicle based on the ACO+FCKF algorithm is shown in FIGURE 5.

In the simulation, the operating conditions of the vehicle are typical double-shifting conditions. The designed vehicle state observer can observe the vehicle status at different speeds. In the simulation, the speed of the car is 80 km/h, the road adhesion coefficient $\mu = 0.85$, the information residual coefficient $\rho = 0.284$, and the sampling interval T = 0.02s. We have the following initial value settings: $\boldsymbol{x_0} = \left[\frac{80}{3.6}, 0, 0, 0, 0, 0.85\right]^T$; $\boldsymbol{P_0} = 0.2 \cdot diag[1, 1, 1, 1, 1, 1]$; $\boldsymbol{Q_0} = 0.1 \cdot diag[1, 1, 1, 1, 1, 1]$; *and* $\boldsymbol{W_0} = 1$. The measurement noise covariance matrix $\mathbf{R}$ takes values of 0.1·diag[1,1,1], 0.05·diag[1,1,1,], 0.01·diag[1,1,1], respectively. Then, we perform three filtering estimation experiments. We can comprehensively derive the optimal input and output membership functions in this paper, as shown in FIGURE 6 and FIGURE 7.

B. VIRTUAL VERIFICATION UNDER FIXED NOISE CONDITIONS

After the optimized input and output membership functions are obtained, it is necessary to indicate the influence of the filtering results before and after optimization by selecting a specific noise covariance. FIGURE 8 shows the driving path set by the car under double-shift line conditions. FIGURE 9 shows the torque output of the front and rear dual motors with respect to time under the simulated conditions.

FIGURES 10, 11, 12, and 13 show the effects of the membership function before and after optimization on the state estimation variables when $\mathbf{R} = 0.05 \cdot \text{diag}[1, 1, 1]$. In each figure, TRUE, FCKF, ACOFCKF are used to represent the actual value of the test vehicle, the fuzzy cubature Kalman filter estimation value, and the ant colony optimization algorithm optimized fuzzy cubature Kalman filter estimation.

Under the condition of fixed noise values, as shown in FIGURES 10, 11, and 12. The influence of the membership function before and after optimization on the longitudinal speed is not obvious. The longitudinal vehicle speed peak error is 4.93%. After optimizing the lateral speed and yaw rate, the tracking curves are closer to the true peak values, and the errors are 6.22% and 3.41%, respectively. They all have deviations within a certain range at different peaks. The reason is that the linear Kalman filter and the linearization approximation error has a certain relationship. FIGURE 13 shows that the estimated value of the adhesion coefficient is faster after optimization, and the estimated peak error is 0.68%, which is closer to the true value.

C. VIRTUAL VERIFICATION UNDER VARIABLE NOISE CONDITIONS

To fully verify the robustness of the optimized algorithm and the effect of the estimation effect on the measurement vector a_y, we added Gaussian white noise that changes with time. The specific change value of the noise is shown in TABLE II, and the noise value is set to a cycle period of 6 s. FIGURE 14 shows a graph of the variation in lateral acceleration after adding the variable noise, which more accurately

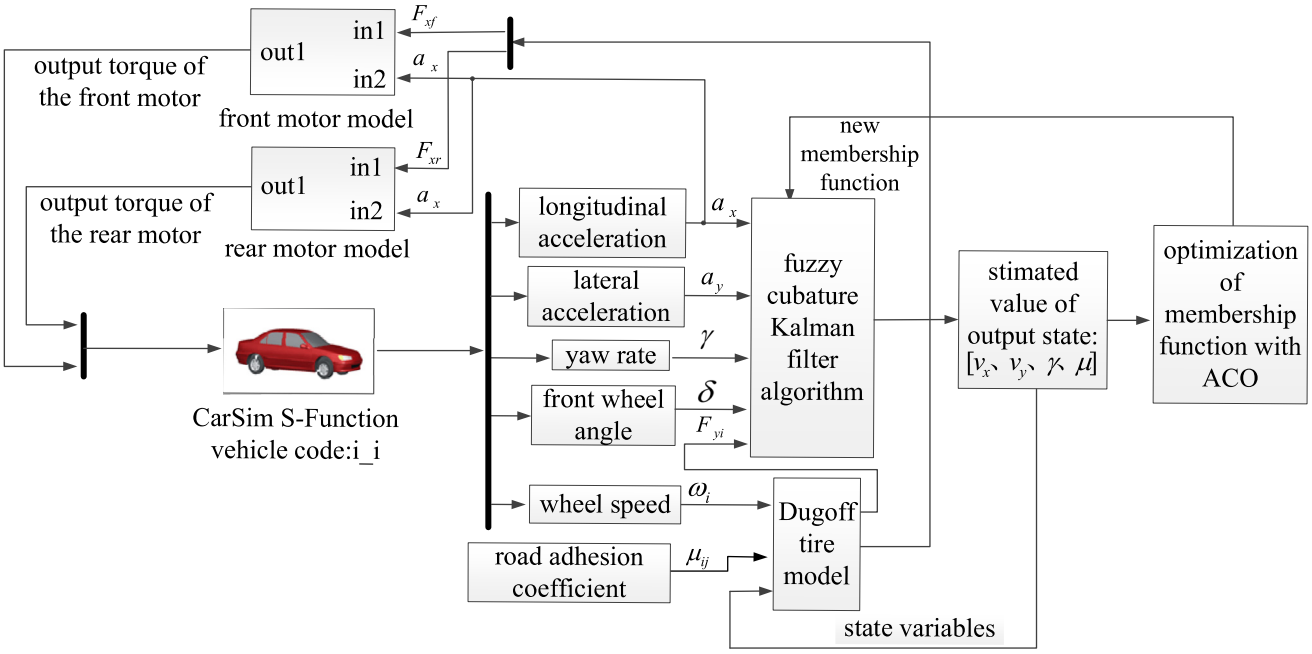

FIGURE 5. CarSim/Simulink cosimulation model.

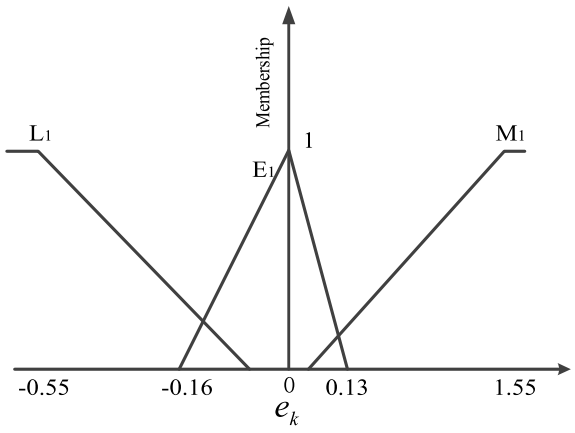

FIGURE 6. Membership function of the optimized input variable.

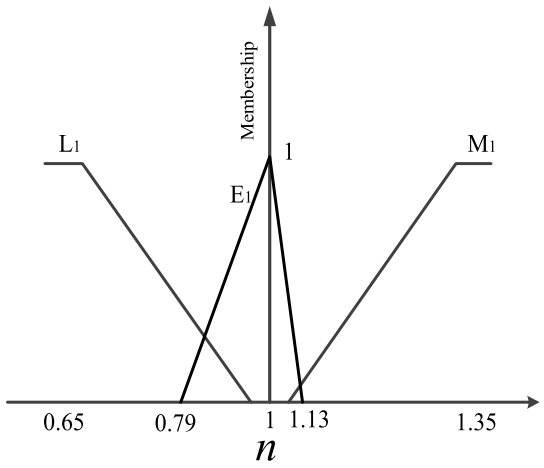

FIGURE 7. Membership function of the optimized output variable.

TABLE 2. Noise variance change table.

Time change sequence	0-2	2-4	4-6	6-8	8-10
Noise variance value	0.04	0.01	0.05	0.04	0.01

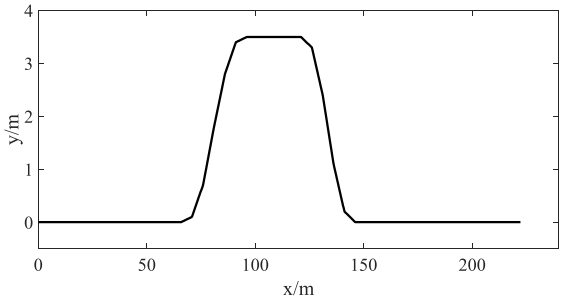

FIGURE 8. Car's driving path.

reflects the influence of noise on the sensor when collecting vehicle information.

After adding variable noise, the estimated results of the car and the critical parts of the road surface are shown in FIGURES 15-18.

We validated the studied vehicle state estimation algorithm by CarSim-Simulink joint simulations. We performed a comparative virtual experiment that compares the fuzzy

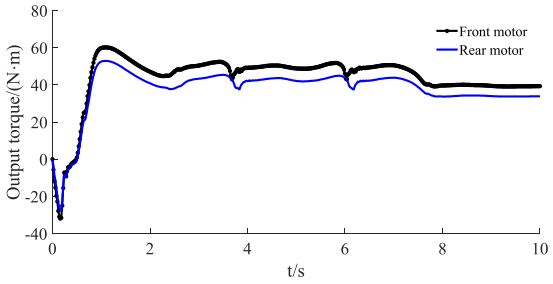

FIGURE 9. Output torque curves of the front and rear motors.

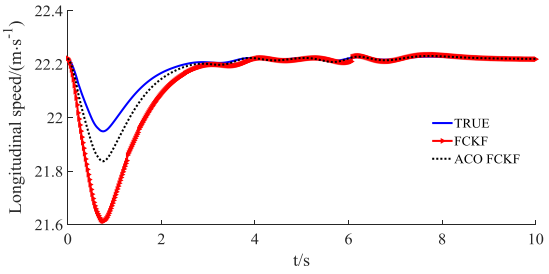

FIGURE 10. Longitudinal speed estimation at constant noise values.

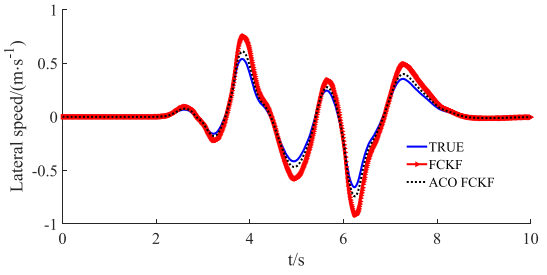

FIGURE 11. Lateral speed estimation at constant noise values.

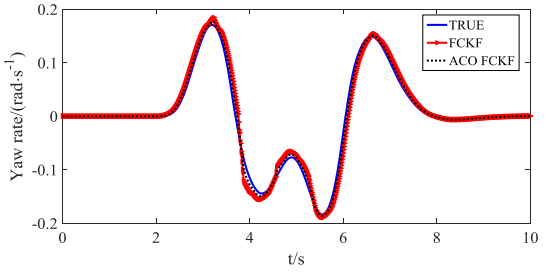

FIGURE 12. Yaw rate estimation at constant noise values.

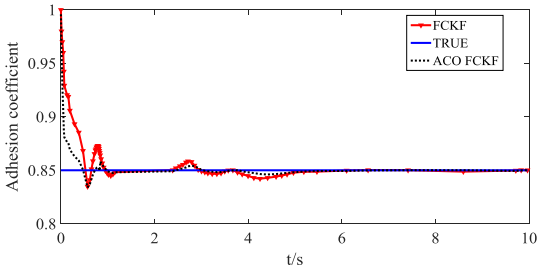

FIGURE 13. Adhesion coefficient estimation at constant noise values.

cubature Kalman filter with the ACOFCKF algorithm. FIGURE 15 shows the longitudinal velocity estimation under double-shifting conditions. The fuzzy cubature Kalman

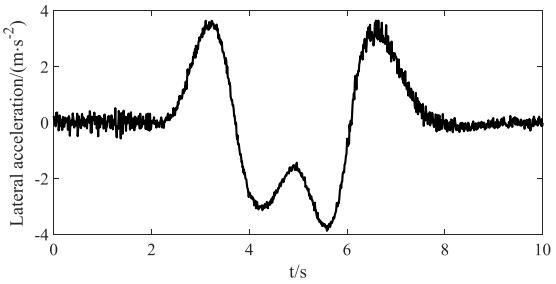

FIGURE 14. Lateral acceleration with variable noise.

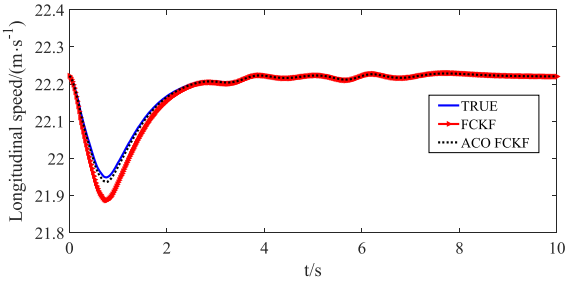

FIGURE 15. Longitudinal speed estimation with variable noise.

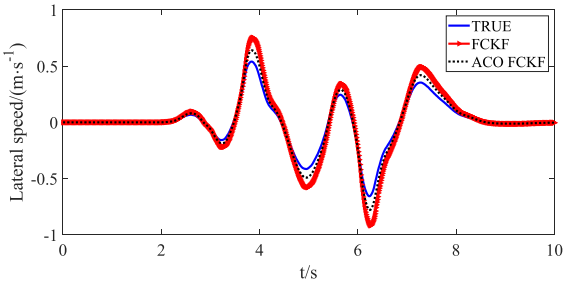

FIGURE 16. Lateral speed estimation with variable noise.

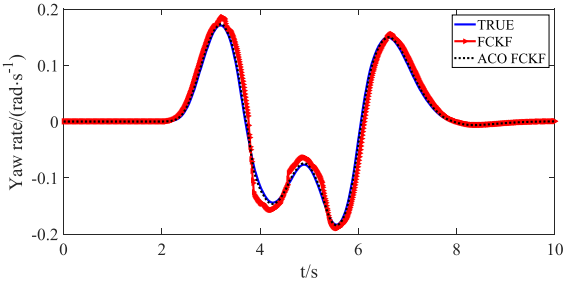

FIGURE 17. Yaw rate estimation with variable noise.

filtering method optimized at the peak is 4.63% better than the preoptimization filtering accuracy. From the estimation of the lateral vehicle speed in FIGURE 16, the fuzzy cubature Kalman filtering method optimized at the peak is improved by 5.38% compared with the preoptimization filtering accuracy. From the yaw angular velocity estimation in FIGURE 17, it can be concluded that the optimized fuzzy cubature Kalman filter method at the peak is improved by 1.06% compared with the preoptimization filtering accuracy. In FIGURE 18,

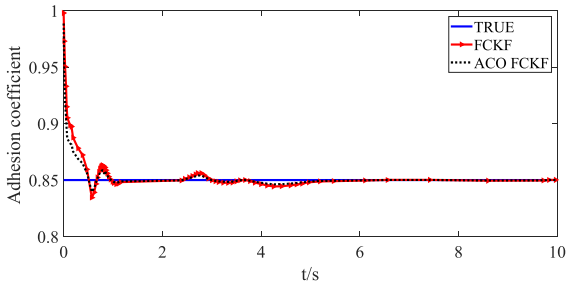

FIGURE 18. Adhesion coefficient estimation with variable noise.

TABLE 3. MAE and RSME indicators of two algorithms under constant noise.

State variables	MAE		RMSE	
	FCKF	ACOFCKF	FCKF	ACOFCKF
Longitudinal speed /(m/s)	0.1286	0.072	0.1449	0.0813
Lateral speed /(m/s)	0.0684	0.0131	0.1108	0.0212
Yaw rate /(rad/s)	0.0081	0.0040	0.0127	0.0063
Adhesion coefficient	0.0188	0.095	0.0373	0.0259

TABLE 4. MAE and RSME indicators of two algorithms under variable noise.

State variables	MAE		RMSE	
	FCKF	ACOFCKF	FCKF	ACOFCKF
Longitudinal speed /(m/s)	0.1321	0.0440	0.1502	0.0500
Lateral speed /(m/s)	0.0514	0.0171	0.0832	0.0277
Yaw rate /(rad/s)	0.0094	0.0018	0.0149	0.0028
Adhesion coefficient	0.0141	0.010	0.0309	0.0240

the estimation of the adhesion coefficient under double-shifting conditions increases the relative error of the estimated value by 0.41%. It can be seen from the above simulation results that the ant colony optimization fuzzy cubature Kalman filter is effective in the double-shift line condition.

In this paper, to more intuitively compare the estimated performance of FCKF and ACOFCKF, we provide the mean absolute error (MAE) index and the mean square error root error (RMSE) index. Obviously, from TABLE 3 and TABLE 4, the MAE index value and the RMSE index value of ACOFCKF are significantly lower than FCKF under both fixed noise conditions and variable noise conditions. Moreover, the estimation accuracy of ACOFCKF is better than that of FCKF.

V. CONCLUSIONS AND FUTURE WORK

In this paper, we first established a three-degree-of-freedom nonlinear vehicle model. Based on the Dugoff tire model and fuzzy logic adaptive cubature Kalman filter theory, a real-time estimation algorithm for the driving state of two-axle electric vehicles was designed. We then used the ant colony algorithm to optimize the fuzzy logic controller, and then we simulated and verified the estimation results before and after optimization under variable noise conditions. According to the optimized algorithm, we can estimate both the vehicle driving state and road surface state information more accurately based on the vehicle sensor information.

First, we proposed an adaptive algorithm for biaxially driven electric vehicle parameter information and state information estimation. The algorithm combines the ant colony algorithm with the FCKF algorithm effectively. The input and output membership functions of the FCKF algorithm are optimized by the optimization function of the ACO algorithm. Compared with the FCKF before optimization, the optimized FCKF further improves the estimation accuracy of the state variables.

Second, we selected the typical double-shift line condition for virtual test comparisons. The results showed that ACOFCKF is still better adaptively adjusted after adding noise, and it can more accurately estimate the state quantity, such as the adhesion coefficient and yaw rate. The algorithm has high stability, strong robustness and better real-time performance.

Future research should mainly build a dSPACE semiphysical simulation system for dual-motor electric vehicles and further verify the actual operation effects of the estimation algorithm through hardware-in-the-loop and real-vehicle tests. After completing the algorithm testing and optimization on the physical hardware system, we will try more parameters of the car and road state estimation, and try to apply the algorithm to the big data environment of the Internet of Vehicles. Then, we can use the new algorithm to process the big data information obtained by a large number of urban vehicle sensors to obtain real-time traffic information for more efficient urban traffic management. Furthermore, we can use this algorithm to better implement IoV-based applications, such as autonomous driving and traffic path planning.

REFERENCES

[1] X. Kong, X. Song, F. Xia, H. Guo, J. Wang, and A. Tolba, "LoTAD: Long-term traffic anomaly detection based on crowdsourced bus trajectory data," *World Wide Web*, vol. 21, no. 3, pp. 825–847, 2018.

[2] X. Kong, M. Li, T. Tang, K. Tian, L. Moreira-Matias, and F. Xia, "Shared subway shuttle bus route planning based on transport data analytics," *IEEE Trans. Autom. Sci. Eng.*, vol. 15, no. 4, pp. 1507–1520, Oct. 2018, doi: 10.1109/TASE.2018.2865494.

[3] D. Zhang and C. K. Yeo, "Optimal handing-back point in mobile data offloading," in *Proc. IEEE Veh. Netw. Conf.*, Nov. 2012, pp. 219–225.
[4] R.-G. Cheng, N.-S. Chen, Y.-F. Chou, and Z. Becvar, "Offloading multiple mobile data contents through opportunistic device-to-device communications," *Wireless Pers. Commun.*, vol. 84, pp. 1963–1979, Oct. 2015.
[5] Z. Lu, X. Sun, and T. La Porta, "Cooperative data offloading in opportunistic mobile networks," in *Proc. IEEE Int. Conf. Comput. Commun. (IEEE INFOCOM)*, Apr. 2016, pp. 1–9.
[6] S. T. Kouyoumdjieva and G. Karlsson, "Energy-aware opportunistic mobile data offloading for users in urban environments," in *Proc. IFIP Netw. Conf. (IFIP Netw.)*, 2015, pp. 1–9.
[7] S.-W. Kim *et al.*, "Cooperative perception for autonomous vehicle control on the road: Motivation and experimental results," in *Proc. IEEE/RSJ Int. Conf. Intell. Robots Syst.*, Nov. 2013, pp. 5059–5066.
[8] D. Zheng, K. Ben, and H. Yuan, "Research of big data space-time analytics for clouding based contexts-aware IOV applications," in *Proc. 2nd Int. Conf. Adv. Cloud Big Data*, 2014, pp. 150–156.
[9] W. Xu *et al.*, "Internet of vehicles in big data era," *IEEE/CAA J. Automatica Sinica*, vol. 5, no. 1, pp. 19–35, Jan. 2018.
[10] L. Guo *et al.*, "A secure mechanism for big data collection in large scale Internet of Vehicle," *IEEE Internet Things J.*, vol. 4, no. 2, pp. 601–610, Feb. 2017.
[11] S. Gugnani, X. Lu, and D. K. Panda, "Performance characterization of hadoop workloads on SR-IOV-enabled virtualized InfiniBand clusters," in *Proc. IEEE/ACM Int. Conf. Big Data Comput.*, Dec. 2016, pp. 36–45.
[12] Z. Zhou, C. Gao, C. Xu, Y. Zhang, S. Mumtaz, and J. Rodriguez, "Social big-data-based content dissemination in Internet of vehicles," *IEEE Trans. Ind. Informat.*, vol. 14, no. 2, pp. 768–777, Feb. 2018.
[13] W. Song and B. Jiang, "Visualization of IoV warning data based on warning velocity association model," in *Proc. IEEE Int. Symp. Comput. Intell. Design*, Dec. 2016, pp. 30–33.
[14] H. Xiong, X. Zhu, and R. Zhang, "Energy recovery strategy numerical simulation for dual axle drive pure electric vehicle based on motor loss model and big data calculation," *Complexity*, vol. 2018, Aug. 2018, Art. no. 4071743. [Online]. Available: https://doi.org/10.1155/2018/4071743
[15] X. J. Kong *et al.*, "Mobility dataset generation for vehicular social networks based on floating car data," *IEEE Trans. Veh. Technol.*, vol. 67, no. 5, pp. 3874–3886, May 2018.
[16] A. Rahim *et al.*, "Vehicular social networks: A survey," *Pervasive Mobile Comput.*, vol. 43, pp. 96–113, Jan. 2018.
[17] L. Wang, L. Zhang, H. Li, Y. Ma, and R. Zhang, "High selective production of 5-hydroxymethylfurfural from fructose by sulfonic acid functionalized SBA-15 catalyst," *Compos. B, Eng.*, vol. 156, pp. 88–94, Jan. 2019.
[18] M. A. Hannan, M. M. Hoque, A. Hussain, Y. Yusof, and P. J. Ker, "State-of-the-art and energy management system of lithium-ion batteries in electric vehicle applications: Issues and recommendations," *IEEE Access*, vol. 6, pp. 19362–19378, 2018.
[19] Z. Tang, A. Liu, and C. Huang, "Social-aware data collection scheme through opportunistic communication in vehicular mobile networks," *IEEE Access*, vol. 4, pp. 6480–6502, 2016.
[20] X. Zhu, Y. Li, D. Jin, and J. Lu, "Contact-aware optimal resource allocation for mobile data offloading in opportunistic vehicular networks," *IEEE Trans. Veh. Technol.*, vol. 6, no. 8, pp. 7384–7399, Aug. 2017.
[21] Y. Li, D. Jin, Z. Wang, L. Zeng, and S. Chen, "Coding or not: Optimal mobile data offloading in opportunistic vehicular networks," *IEEE Trans. Intell. Transp. Syst.*, vol. 15, no. 1, pp. 318–333, Feb. 2014.
[22] L. Wang, L. Liu, X. Cao, X. Tian, and Y. Cheng, "Sociality-aware resource allocation for device-to-device communications in cellular networks," *IET Commun.*, vol. 9, no. 3, pp. 342–349, 2015.
[23] T. S. J. Darwish and K. A. Bakar, "Fog based intelligent transportation big data analytics in the Internet of vehicles environment: Motivations, architecture, challenges, and critical issues," *IEEE Access*, vol. 6, pp. 15679–15701, 2018.
[24] G. Dimitrakopoulos, "Intelligent transportation systems based on Internet-connected vehicles: Fundamental research areas and challenges," in *Proc. Int. Conf. Telecommun.*, 2011, pp. 145–151.
[25] J. A. Guerrero-Ibanez, S. Zeadally, and J. Contreras-Castillo, "Integration challenges of intelligent transportation systems with connected vehicle, cloud computing, and Internet of Things technologies," *IEEE Wireless Commun.*, vol. 22, no. 6, pp. 122–128, Dec. 2015.
[26] W. Liu, S.-W. Kim, K. Marczuk, and M. H. Ang, "Vehicle motion intention reasoning using cooperative perception on urban road," in *Proc. IEEE Int. Conf. Intell. Transp. Syst.*, Oct. 2014, pp. 424–430.
[27] W. Liu, S. W. Kim, Z. J. Chong, X. T. Shen, and M. H. Ang, "Motion planning using cooperative perception on urban road," in *Proc. IEEE Robot., Automat. Mechatronics*, Nov. 2013, pp. 130–137.
[28] S.-W. Kim *et al.*, "Vehicle autonomy using cooperative perception for 594 mobility-on-demand systems," in *Motion and Operation Planning of 595 Robotic Systems*. Berlin, Germany: Springer, 2015.
[29] S.-W. Kim, W. Liu, M. H. Ang, E. Frazzoli, and D. Rus, "The impact of cooperative perception on decision making and planning of autonomous vehicles," *IEEE Intell. Transp. Syst. Mag.*, vol. 7, no. 3, pp. 39–50, Jul. 2015.
[30] S.-W. Kim *et al.*, "Multivehicle cooperative driving using cooperative perception: Design and experimental validation," *IEEE Trans. Intell. Transp. Syst.*, vol. 16, no. 2, pp. 663–680, Apr. 2015.
[31] L. Yang, B. Wang, R. Zhang, H. Zhou, and R. Wang, "Analysis on location accuracy for the binocular stereo vision system," *IEEE Photon. J.*, vol. 10, no. 1, Feb. 2018, Art. no. 7800316.
[32] Z. Wang *et al.*, "Vehicle system state estimation based on adaptive unscented Kalman filtering combing with road classification," *IEEE Access*, vol. 5, pp. 27786–27799, 2017.
[33] B. Ma, D. Wang, S. Cheng, and X. Xie, "Modeling and analysis for vertical handoff based on the decision tree in a heterogeneous vehicle network," *IEEE Access*, vol. 5, pp. 8812–8824, 2017.
[34] Y. Xu, Y. S. Shmaliy, Y. Li, and X. Chen, "UWB-based indoor human localization with time-delayed data using EFIR filtering," *IEEE Access*, vol. 5, pp. 16676–16683, 2017.
[35] F. Lu, Y. Huang, J. Huang, and X. Qiu, "A hybrid Kalman filtering approach based on federated framework for gas turbine engine health monitoring," *IEEE Access*, vol. 6, pp. 9841–9853, 2017.
[36] X. Liu, B. Chen, H. Zhao, J. Qin, and J. Cao, "Maximum correntropy Kalman filter with state constraints," *IEEE Access*, vol. 5, pp. 25846–25853, 2017.
[37] G. F. Basso, T. G. S. De Amorim, A. V. Brito, and T. P. Nascimento, "Kalman filter with dynamical setting of optimal process noise covariance," *IEEE Access*, vol. 5, pp. 8385–8393, 2017.
[38] M. Shi, D. Li, and J. Q. Zhang, "An alternating Bayesian approach to PARAFAC decomposition of tensors," *IEEE Access*, vol. 6, pp. 36487–36499, 2018.
[39] R.-H. Zhang, Z.-C. He, H.-W. Wang, F. You, and K.-N. Li, "Study on self-tuning tyre friction control for developing main-servo loop integrated chassis control system," *IEEE Access*, vol. 5, pp. 6649–6660, 2017.
[40] X. Sun, H. Zhang, W. Meng, R. Zhang, K. Li, and T. Peng, "Primary resonance analysis and vibration suppression for the harmonically excited nonlinear suspension system using a pair of symmetric viscoelastic buffers," *Nonlinear Dyn.*, vol. 94, no. 2, pp. 1243–1265, 2018.
[41] L.-H. Zhao, Z.-Y. Liu, and H. Chen, "Design of a nonlinear observer for vehicle velocity estimation and experiments," *IEEE Trans. Control Syst. Technol.*, vol. 19, no. 3, pp. 664–672, May 2011.
[42] S. Han and K. Huh, "Monitoring system design for lateral vehicle motion," *IEEE Trans. Veh. Technol.*, vol. 60, no. 4, pp. 1394–1403, May 2011.
[43] X. J. Jin and G. Yin, "Estimation of lateral tire–road forces and sideslip angle for electric vehicles using interacting multiple model filter approach," *J. Franklin Inst.*, vol. 352, no. 2, pp. 686–707, 2015.
[44] D. W. Pi, N. Chen, J. X. Wang, and B. J. Zhang, "Design and evaluation of sideslip angle observer for vehicle stability control," *Int. J. Automot. Technol.*, vol. 12, p. 391, Jun. 2011.
[45] J. Yoon and B. Kim, "Vehicle position estimation using tire model," in *Information Science and Applications* (Lecture Notes in Electrical Engineering), vol. 339. Berlin, Germany: Springer, 2015, pp. 761–768.
[46] K. Alipour and S. A. A. Moosavian, "Effect of terrain traction, suspension stiffness and grasp posture on the tip-over stability of wheeled robots with multiple arms," *Adv. Robot.*, vol. 26, nos. 8–9, pp. 817–842, 2012.
[47] J. Villagra, B. d'Andréa-Novel, M. Fliess, and H. Mounier, "A diagnosis-based approach for tire–road forces and maximum friction estimation," *Control Eng. Pract.*, vol. 19, no. 2, pp. 174–184, 2011.
[48] C. Senabre, E. Velasco, and S. Valero, "Comparative analysis of vehicle brake data in the ministry of transport test on the roller brake tester and on flat ground," *Int. J. Automot. Technol.*, vol. 13, no. 5, pp. 735–742, 2012.
[49] S. J. Kim, K.-S. Kim, and Y.-S. Yoon, "Development of a tire model based on an analysis of tire strain obtained by an intelligent tire system," *Int. J. Automot. Technol.*, vol. 16, pp. 865–875, Oct. 2015.
[50] J. Zarei and E. Shokri, "Nonlinear and constrained state estimation based on the cubature Kalman filter," *Ind. Eng. Chem. Res.*, vol. 53, no. 10, pp. 3938–3949, 2014.

[51] S. Bououden, M. Chadli, and H. R. Karimi, "An ant colony optimization-based fuzzy predictive control approach for nonlinear processes," *Inf. Sci.*, vol. 299, pp. 143–158, Apr. 2015.
[52] H. Xiong *et al.*, "A new synchronous control method for dual motor electric vehicle based on cognitive-inspired and intelligent interaction," *Future Gener. Comput. Syst.*, vol. 94, pp. 536–548, May 2019.

HUIYUAN XIONG was born in Hubei, China, in 1973. He received the M.S. degree in mechanical design and theory from the Huazhong University of Science and Technology, China, in 2003, and the Ph.D. degree in engineering mechanics from Sun Yat-sen University, China, in 2009, where he has been an Associate Professor with the Graduate School, since 2012. His research interests include design theory and method of electric vehicles, integrated optimization technology for powertrain of electric vehicle, and hardware in the loop simulation.

JIANXUN LIU was born in Cangzhou, Hebei, China, in 1996. He received the B.S. degree from the College of Mechanical Science and Engineering, Huazhong University of Science and Technology, China, in 2016. He is currently pursuing the M.S. degree with Sun Yat-sen University. He conducted research on new energy electric vehicle, the optimal control of electric vehicle, and intelligent recognition and control.

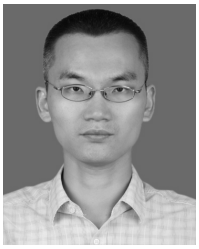

RONGHUI ZHANG received the B.Sc. (Eng.) degree from the Department of Automation Science and Electrical Engineering, Hebei University, Baoding, China, in 2003, the M.S. degree in vehicle application engineering from Jilin University, Changchun, China, in 2006, and the Ph.D. (Eng.) degree in mechanical and electrical engineering from the Changchun Institute of Optics, Fine Mechanics and Physics, Chinese Academy of Sciences, Changchun, in 2009. After finishing his Postdoctoral research work at INRIA, Paris, France, in 2011, he is currently a Research Fellow with the Research Center of Intelligent Transportation Systems, School of Intelligent Systems Engineering, Sun Yat-sen University, Guangzhou, Guangdong, China. He has published more than 20 papers in international journals. His current research interests include computer vision, intelligent control, and ITS.

XIONGLAI ZHU was born in Jiangxi, China, in 1994. He received the B.S. degree from the College of Traffic and Transportation, Chongqing Jiaotong University, China, in 2016. He is currently pursuing the M.S. degree with Sun Yat-sen University. He conducted research on energy feedback of electric vehicle and optimal control of motors.

HUAN LIU was born in Jiangxi, China, in 1996. She received the B.S. degree from the College of Mechanical and Electrical Engineering, Northeast Forestry University, China, in 2018. She is currently pursuing the M.S. degree with Sun Yat-sen University. She conducted research on new energy electric vehicle and the optimal control of electric vehicle.